Single-Molecule Protein Detection in a Biofluid Using a Quantitative Nanopore Sensor

Avinash Kumar Thakur[†,‡] and Liviu Movileanu*[,†,‡,§]

[†]Department of Physics, Syracuse University, 201 Physics Building, Syracuse, New York 13244-1130, United States

[‡]Structural Biology, Biochemistry, and Biophysics Program, Syracuse University, 111 College Place, Syracuse, New York 13244-4100, United States

[§]Department of Biomedical and Chemical Engineering, Syracuse University, 329 Link Hall, Syracuse, New York 13244, United States

Ⓢ *Supporting Information*

ABSTRACT: Protein detection in complex biological fluids has wide-ranging significance across proteomics and molecular medicine. Existing detectors cannot readily distinguish between specific and nonspecific interactions in a heterogeneous solution. Here, we show that this daunting shortcoming can be overcome by using a protein bait-containing biological nanopore in mammalian serum. The capture and release events of a protein analyte by the tethered protein bait occur outside the nanopore and are accompanied by uniform current openings. Conversely, nonspecific pore penetrations by nontarget components of serum, which take place inside the nanopore, are featured by irregular current blockades. As a result of this unique peculiarity of the readout between specific protein captures and nonspecific pore penetration events, our selective sensor can quantitatively sample proteins at single-molecule precision in a manner distinctive from those employed by prevailing methods. Because our sensor can be integrated into nanofluidic devices and coupled with high-throughput technologies, our approach will have a transformative impact in protein identification and quantification in clinical isolates for disease prognostics and diagnostics.

KEYWORDS: FhuA, ion channel, protein−protein interface, protein dynamics, stochastic sensing, electrophysiology, membrane protein engineering
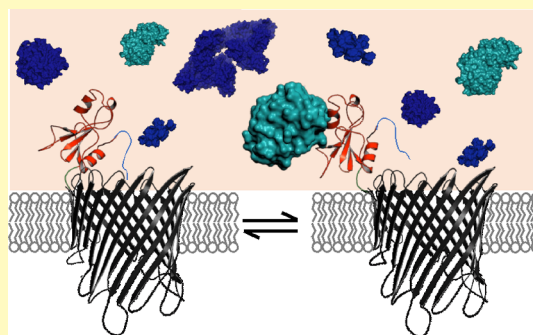
A current challenge in personalized medicine is the ability to detect proteins in a specific, sensitive, and scalable fashion using biofluids.[1,2] The prevailing methods for protein analysis in vitro, such as biolayer interferometry, surface plasmon resonance, and isothermal titration calorimetry, are usually employed in homogeneous samples. Yet, these approaches cannot be used in a heterogeneous solution, because of nonspecific protein binding and a deteriorated signal-to-noise ratio (SNR). In the past decade, significant progress has been made in developing alternative bioanalytical approaches for detecting proteins and their interactions in complex biofluids.[3−8] Conventional techniques, such as mass spectrometry, enzyme-linked immunosorbent assay, and Western Blot, have facilitated detection and exploration of proteins in biofluids. Here, we demonstrate accurate determination of protein detection in mammalian serum at single-molecule precision using a modular pore-based nanostructure. By using conventional nanopore sensors, it is difficult to distinguish signals generated by specific interactions with the target protein from those generated by nonspecific pore penetrations of other constituents of a heterogeneous sample. This challenge is exacerbated in nanopore recordings, because both specific and nonspecific events appear as current

blockades. Therefore, pore penetration by biofluid constituents enhances the susceptibility for sampling false capture events and precludes accurate protein detection.

In this work, we show that this persistent limitation can be overcome by detecting the protein analyte outside the nanopore by means of a tethered protein bait (Figure 1a). The 455-residue single-polypeptide chain protein nanopore, also named t-FhuA,[9,10] is an extensive truncation of ferric hydroxamate uptake component A (FhuA)[11] of *Escherichia coli*. This is a robust monomeric β-barrel.[12−15] The protein bait was engineered at the N terminus of t-FhuA via a flexible hexapeptide tether ((GGS)$_2$). As a test case for the protein bait and protein analyte, we used 110-residue RNase barnase (Bn)[16] and its 89-residue inhibitor barstar (Bs),[17,18] respectively. The pivotal mechanism of this sensing approach in fetal bovine serum (FBS) is the transduction of protein capture and release events into a high-fidelity electrical readout via a movable polypeptide adaptor (O), which was fused to the
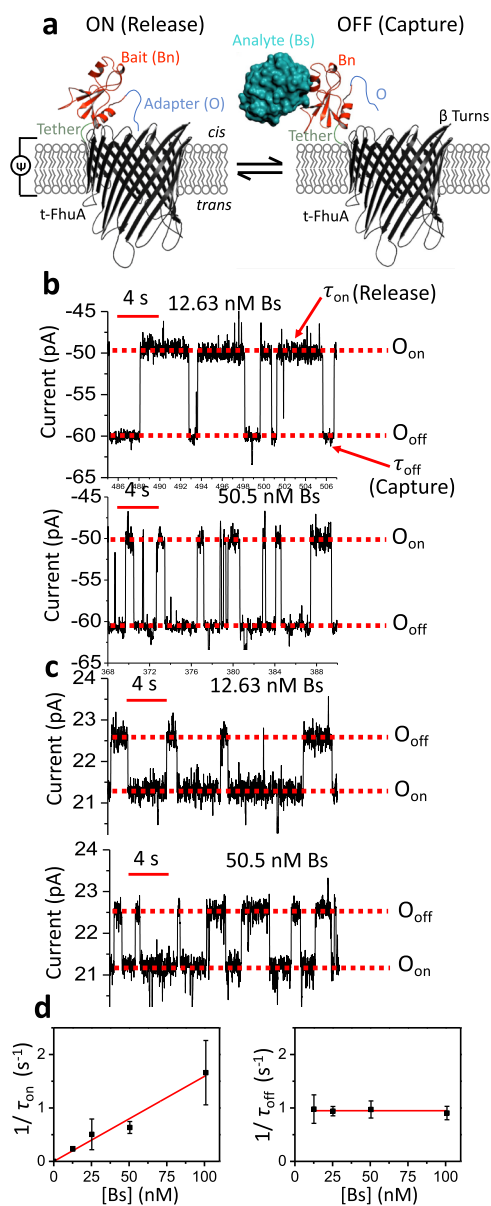
Figure 1. Single-molecule protein detection at single-tethered receptor resolution. (a) Stochastic protein sensing of barstar (Bs) protein using $OBn(GGS)_2t$-FhuA. This protein sensor encompasses a truncated t-FhuA protein pore, a short $(GGS)_2$ hexapeptide tether, a barnase (Bn) protein receptor, and a dodecapeptide adapter (O). This model was generated in Pymol using the pdb files 1BY3 and 1BRS for (FhuA)[11] and (Bn−Bs),[18] respectively. (b) Representative single-channel electrical traces of $OBn(GGS)_2t$-FhuA in the presence of 12.63 nM Bs (top) and 50.5 nM Bs (bottom) at an applied transmembrane potential of −40 mV. The control experiment in the absence of Bs is shown in Supporting Information, Figure S1. Single-channel electrical traces were further processed using a 20 Hz low-pass 8-pole Bessel filter. O_{on} indicates the Bs-released open substate; O_{off} shows the Bs-captured open substate. (c) Representative single-channel electrical traces of $OBn(GGS)_2t$-FhuA in the presence of 12.63 nM Bs (top) and 50.5 nM Bs (bottom) at an applied transmembrane potential of +15 mV. The control experiment in the absence of Bs is shown in Supporting Information, Figure S6. Single-channel electrical traces were further processed using a 20 Hz low-pass 8-pole Bessel filter. O_{on} and O_{off} have the same meanings as those stated in (b). (d) Both diagrams show dependence of $1/\tau_{on}$ (left) and $1/\tau_{off}$ (right) on Bs concentration, [Bs]. Here, these kinetic rate constants in the form of mean ± s.e.m. are $k_{on} = (1.59 \pm 0.09) \times 10^7$

Figure 1. continued

$M^{-1} s^{-1}$ and $k_{off} = 0.95 \pm 0.02\ s^{-1}$. Data points in both panels represent mean ± s.d. obtained from n distinct experiments. In this case, n was 5, 3, 3, and 4, for a [Bs] of 12.63, 25.25, 50.5, and 100.01 nM, respectively. Experimental conditions in (d) were the same as those stated in (c).

untethered end of the bait. Therefore, our single-polypeptide chain protein sensor is $OBn(GGS)_2t$-FhuA, a 583-residue pore-based nanostructure.

Our selective nanopore sensor permits single-channel electrical recordings[12,19] over long periods under these challenging conditions. In this work, specific protein captures, which occur outside the nanopore, lead to uniform current openings. In contrast, the FBS constituents, which partition into the t-FhuA pore lumen, bring about irregular current blockades. This readout feature makes the protein captures unambiguously different from those events resulting from nonspecific pore penetrations of nontarget FBS constituents. This strategy for distinguishing between protein captures and releases from other nonspecific residual events is a fundamental distinction of this work from prior detection studies using conventional nanopores in homogeneous solutions.[1,20−37] Here, we hypothesized that the SNR value might be further amplified under optimized recording conditions. Moreover, we show that time-resolved protein capture and release events can be recorded in a heterogeneous solution at an applied potential as low as 15 mV, because of a satisfactory SNR value. Yet, in these challenging circumstances the bait-analyte complex formation followed a simple bimolecular association process, whereas the analyte release underwent a unimolecular dissociation process. Such a membrane protein design, which makes this method highly specific and quantitative, enables accurate determinations of single-molecule protein detection in FBS. Finally, the kinetics of binding and unbinding in a heterogeneous solution was identical to those determined in a homogeneous solution, confirming that specific and nontarget single-molecule events are independent of each other.

■ RESULTS

Maximization of the SNR Value in FBS. Our aim was to record single protein captures at a maximized SNR and at minimized interference of FBS-induced current transitions. $OBn(GGS)_2t$-FhuA spontaneously inserted itself from the cis side into the membrane with a preferred orientation (Figure 1a). At a transmembrane potential of −40 mV with respect to the cis side (grounded) and in 300 mM KCl, 10 mM Tris-HCl, pH 8.0, $OBn(GGS)_2t$-FhuA showed a uniform single-channel current with a mean value of −46.9 ± 2.5 pA ($n = 4$ experiments) (Supporting Information, Figure S1). When Bs was added to the cis side at a low nanomolar Bs concentration, [Bs], transient current transitions were readily observed between O_{on} and O_{off} (Figure 1b). The current amplitudes of these open substates were −47.5 ± 2.1 pA ($n = 4$) and −58.2 ± 3.1 pA ($n = 4$), respectively. We have recently shown that these current transitions represent reversible release (O_{on}) and capture (O_{off}) events of Bs by Bn.[10] We used a single-site mutant of Bn (H102A), a catalytically inactive protein bait. In this way, we examined more weakly binding protein captures (e.g., K_d of 10^{-9} M)[10,38] than strongly binding protein captures (e.g., wild-type Bn, K_d of ∼10^{-14} M).[38] This tactic permitted
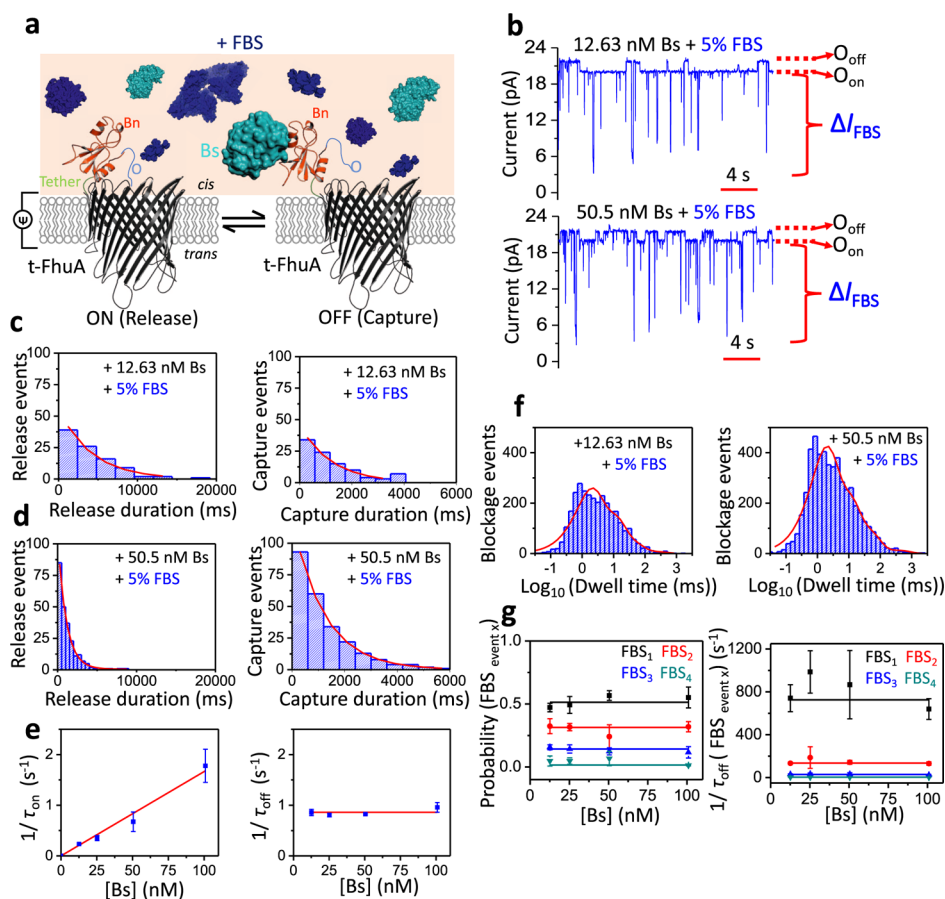
Figure 2. Single-molecule protein detection at single-tethered receptor resolution in unprocessed FBS. (a) Schematic representation of stochastic protein sensing of Bs using $OBn(GGS)_2$t-FhuA in the presence of FBS. (b) Representative single-channel electrical traces of $OBn(GGS)_2$t-FhuA in 5% (v/v) FBS and in the presence of 12.63 nM Bs (top) and 50.5 nM Bs (bottom). Experiments were conducted at an applied transmembrane potential of +15 mV. Single-channel electrical traces were further processed using a 20 Hz low-pass 8-pole Bessel filter. Bs was added to the cis side of the chamber. O_{on} and O_{off} stand for the same meanings as in Figure 1a. Single-molecule protein captures are indicated by upward current transitions (to O_{off}) from the basal current level (O_{on}) of $OBn(GGS)_2$t-FhuA. ΔI_{FBS} represents a spectrum of FBS-induced current transitions either departed from either O_{on} or O_{off} substate. (c) Representative standard histograms of the release (τ_{on}; left) and capture (τ_{off}; right) durations at 12.63 nM Bs. The τ_{on} and τ_{off} values obtained from the fits (mean ± s.e.m.) were 4188 ± 429 ms ($n = 96$) and 1220 ± 90 ms ($n = 97$), respectively. (d) Representative standard histograms of the release (τ_{on}; left) and capture (τ_{off}; right) durations at 50.5 nM Bs. The τ_{on} and τ_{off} values obtained from the fits were 1150 ± 57 ms ($n = 239$) and 1223 ± 25 ms ($n = 243$), respectively. Experimental conditions in (c,d) were the same as in (b). (e) Dependence of $1/\tau_{on}$ (left) and $1/\tau_{off}$ (right) on [Bs] when measurements were conducted in 5% FBS. Here, $k_{on} = (1.67 \pm 0.09) \times 10^7 M^{-1} s^{-1}$ and $k_{off} = 0.86 \pm 0.03 s^{-1}$. Data points in both panels represent mean ± s.d. obtained from $n = 3$ distinct experiments. (f) Event dwell time histograms of FBS-induced current blockades in 5% (v/v) FBS as well as in the presence of 12.63 nM Bs (left) and 50.5 nM Bs (right). The numbers of FBS-induced events were 3040 and 5007, respectively. The best-fit model was a multiexponential function with four terms (Supporting Information, Tables S4−S5). (g) Event probability (left) and dwell time (right) values of FBS-induced current blockades ($FBS_{event\,x}$) are independent of [Bs]. Data points in both panels represent mean ± s.d. obtained from $n = 3$ distinct experiments. Experimental conditions in panels (c−g) were the same as those stated in (b).

the recording of single-molecule Bs capture events at equilibrium. The O_{off} and O_{on} current amplitudes enabled a clear signal separation of ∼10 pA for the capture and release events, respectively. Enhancing the Bs concentration increased the event frequency (Figure 1b). Standard histograms of the release (τ_{on}) and capture (τ_{off}) durations are presented in the Supporting Information (Figure S2). The statistically significant fit model was determined by using a standard logarithm likelihood ratio (LLR) test.[39] At a confidence level $C = 0.95$, the best model was one-exponential fit, unless otherwise stated (see below terms resulting from serum constituents). This outcome suggests single-barrier transitions of the free-energy landscape of these single-molecule protein capture and release events. However, the incubation of the cis side of the chamber in FBS within the range of 1−5% (v/v) FBS resulted in the

appearance of large-current amplitude and long-lived blockades at a transmembrane potential of −40 mV (Supporting Information, Figure S3). For example, at an FBS concentration of 5% (v/v), the duration of some of these long-lived events was even longer than 10 s.

Therefore, these long-lived FBS-induced events interfered with our ability to detect single-molecule protein captures. t-FhuA is an acidic β-barrel (P_K/P_{Cl} is ∼5.5).[13] Thus, the pore lumen acts as an energetic barrier for the partitioning of negatively charged FBS constituents. In contrast, positively charged FBS impurities are electrostatically attracted into the pore interior. A negative transmembrane potential would amplify this process, because FBS was added to the cis side of the chamber. On the other hand, a positive transmembrane potential would counteract on positive FBS constituents,

whereas the negatively charged FBS impurities would face an energetic barrier due to the cation selectivity of t-FhuA. These outcomes led us to systematically examine the voltage dependence of the differential current, ΔI_{off-on} $[I(O_{off}) - I(O_{on})]$, between the capture and release substates. For example, at a negative voltage bias, ΔI_{off-on} was ~17.6 and ~2.5 pA at −50 and −15 mV, respectively (Supporting Information, Figure S4). This inspection revealed greater ΔI_{off-on} values for negative potentials than those values recorded at positive potentials. For example, ΔI_{off-on} spanned at a range of 1.2−1.8 pA between +15 and +40 mV, respectively. This finding motivated us to conduct our single-molecule protein capture measurements at a higher positive potential. Surprisingly, we noted that an increase in the positive voltage bias at a value of +40 mV deteriorated the SNR and induced transient current fluctuations in the stability of the substates O_{on} and O_{off} (Supporting Information, Figure S5).

Therefore, we then tested single-molecule Bs captures at a potential of +15 mV. In these conditions, $OBn(GGS)_2t$-FhuA exhibited a uniform unitary current of 19.9 ± 1.5 pA ($n = 5$) (Supporting Information, Figure S6). When Bs was added to the cis side at a low-nanomolar concentration, reversible protein captures in the form of transient current transitions were noted between O_{on} and O_{off}. The mean currents of these open substates were 20.1 ± 1.6 pA ($n = 5$) and 21.3 ± 1.5 pA ($n = 5$), respectively. This results in a ΔI_{off-on} of ~1.2 ± 0.1 pA ($n = 5$). Representative single-channel traces of these protein captures, when either 12.63 nM Bs (top trace) or 50.5 nM Bs (bottom trace) was added to the cis side, are illustrated in Figure 1c. Standard histograms of the release (τ_{on}) and capture (τ_{off}) durations are presented in the Supporting Information (Figure S7).

Time analyses of these events were used to determine the association (k_{on}) and dissociation (k_{off}) rate constants of the Bn−Bs interactions, where $k_{on} = 1/([Bs]\tau_{on})$ and $k_{off} = 1/\tau_{off}$. Here, τ_{on} and τ_{off} denote the release and capture durations of the free Bs by the tethered Bn, respectively. The frequency of the single Bs captures in the form of $1/\tau_{on}$ was linearly dependent on [Bs], suggesting a bimolecular association process (Figure 1d). The slope of the linear fit of event frequency was k_{on}, with a mean value of $(1.59 ± 0.09) \times 10^7$ M^{-1} s^{-1}. The reciprocal of the τ_{off} duration, k_{off}, with a mean value of 0.95 ± 0.02 s^{-1}, was independent of [Bs], indicating a unimolecular dissociation process (Supporting Information, Table S1). These values correspond to a K_d of 60 ± 4 nM (Supporting Information, Table S2). The kinetic and equilibrium constants determined at +15 mV were in excellent accord with those parameters obtained in an earlier study at a voltage bias of −40 mV ($k_{on} = (1.34 ± 0.04) \times 10^7$ M^{-1} s^{-1}, $k_{off} = 0.86 ± 0.02$ s^{-1}, and $K_d = 64 ± 02$ nM).[10] These values are also in agreement with prior bulk-phase kinetic determinations.[16,38] Furthermore, k_{on} and k_{off} were not sensitive to changes in the transmembrane potential when the voltage bias was negative (Supporting Information, Figure S8).

Single-Molecule Protein Detection in FBS. Based upon the above findings, we then examined single-molecule Bs captures at a transmembrane potential of +15 mV and in the presence of 5% (v/v) FBS (Figure 2a). Under these conditions, FBS-induced current blockades were in the range of milliseconds. Two representative single-channel traces were shown when either 12.63 nM Bs (top trace) or 50.5 nM Bs

(bottom trace) was added to the cis side (Figure 2b). FBS-induced large-amplitude blockades featured a current amplitude (ΔI_{FBS}) of 17.2 ± 1.2 pA ($n = 3$). These current blockades were unambiguously distinguished from specific Bs capture-induced, low-amplitude current transitions between the O_{on} and O_{off} substates (ΔI_{off-on} was 1.4 ± 0.3 pA ($n = 3$)). We highlight that single-molecule Bs captures were detected outside the nanopore, whereas the nonspecific FBS-induced events were probed inside the nanopore. Therefore, we hypothesize that these two categories of events are independent of each other. Indeed, we noticed that any reversible, large-amplitude, FBS-induced current transition departing from either O_{on} or O_{off} substate always returned to the same substate. This confirms their independent mechanisms.

Histograms of the release and capture durations in the presence of 5% (v/v) FBS, and at either 12.63 or 50.5 nM Bs, are displayed in Figure 2c,d, respectively. Remarkably, the presence of FBS did not affect single-exponential distributions of these time constants. Moreover, $(1/\tau_{on})$ was linearly dependent on [Bs], whereas $(1/\tau_{off})$ was independent of [Bs], suggesting that these events resulted from a bimolecular association process and a unimolecular dissociation mechanism in the presence of FBS. Again, k_{on} and k_{off} of the single-molecule protein captures were determined in the presence of FBS using linear fits of the dependences of $1/\tau_{on}$ ([Bs]) and $1/\tau_{off}$ ([Bs]) (Figure 2e; Supporting Information, Table S3). These values were $(1.67 ± 0.09) \times 10^7$ M^{-1} s^{-1} and 0.86 ± 0.03 s^{-1}, respectively, which corresponded to a K_d of 52 ± 3 nM (Supporting Information, Table S2). Remarkably, these kinetic and equilibrium constants determined in FBS are closely similar to those acquired in a homogeneous solution. This outcome is significant, because it also reveals that no FBS impurity interacts with the binding interface of either Bn or Bs. To test whether the presence of Bs affected the partitioning of nontarget FBS constituents into the pore lumen, we conducted the time analysis of the large-amplitude current transitions (I_{FBS}) at [Bs] in the range of 0−100 nM. For the time analysis of the Bn−Bs interactions, we used a 20 Hz low-pass Bessel filter. Yet, in the case of the FBS-induced current blockades, an 0.5 kHz filter frequency was employed (Supporting Information, Figure S9), which corresponded to an event deadtime, T_d, of 0.36 ms.[40] An LLR test analysis indicated that the FBS-induced events followed a four-exponential distribution, regardless of [Bs] (Figure 2f,g; Supporting Information, Tables S4−S9). We conclude that the Bn−Bs interactions are also quantitatively independent of the FBS-induced current blockades.

Single-Molecule Protein Detection in Heat-Inactivated FBS. The enhancement of protein-detection sensitivity might also be achieved by reducing the highly frequent and short-lived current blockades produced by the FBS impurities. Studies of protein detection using other bioanalytical methods show that the inhibition of background noise is usually conducted either by gradual dilutions or by heat inactivation (HI) of the serum.[41−44] Here, we examined single-molecule Bs captures by the tethered Bn when heat-inactivated FBS (HI-FBS) was added in increased volumetric concentrations. Two single-channel traces are illustrated when either 5% (v/v) HI-FBS (top trace) or 10% (v/v) HI-FBS (bottom trace) were added to the cis side at 12.63 nM Bs (Figure 3a; Supporting Information, Figure S10). Again, concurrent Bs capture-induced, low-amplitude current transitions (ΔI_{off-on}) and HI-
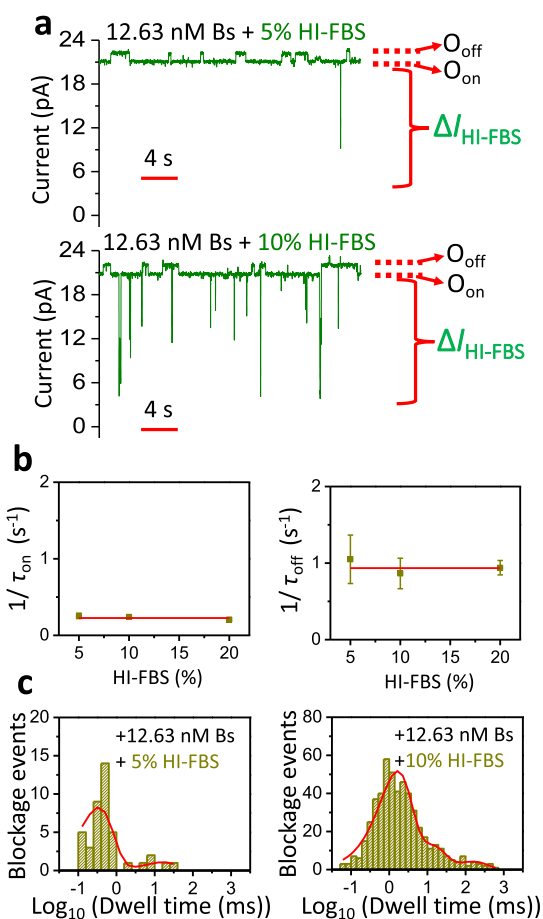
Figure 3. Single-molecule protein detection in HI-FBS. (a) Single-channel electrical traces of OBn(GGS)$_2$t-FhuA in either 5% (v/v) (top) or 10% (bottom) HI-FBS and in the presence of 12.63 nM Bs. The applied transmembrane potential was +15 mV. Single-channel electrical traces were further processed using a 20 Hz low-pass 8-pole Bessel filter. Bs was added to the cis side of the chamber. O$_{on}$ and O$_{off}$ have the same meanings as in Figure 1a. ΔI_{HI-FBS} represents a spectrum of HI-FBS-induced current transitions. (b) Dependence of $1/\tau_{on}$ (left) and $1/\tau_{off}$ (right) on the HI-FBS concentration. Linear fits of both plots provide evidence that the average of $1/\tau_{on}$ and $1/\tau_{off}$ of the Bs captures at 12.63 nM Bs are independent of the tested HI-FBS concentration. Here, $1/\tau_{on}$ = 0.227 ± 0.014 s^{-1} and $1/\tau_{off}$ = 0.934 ± 0.030 s^{-1}. Data points represent mean ± s.d. obtained from n = 3 distinct experiments. Experimental conditions in panel (b) were the same as those stated in (a). (c) Dwell time histograms of HI-FBS-induced current blockades in either 5% (left) or 10% HI-FBS (right), and in the presence of 12.63 nM Bs. The number of HI-FBS-induced events were 42 and 515, respectively. For the top graph, the best fit model was a double-exponential distribution function with corresponding dwell time and probability values (mean ± s.e.m.), as follows: τ_{off-1} = 0.33 ± 0.23 ms, P_1 = 0.88 ± 0.14, τ_{off-2} = 16.57 ± 2.09 ms, P_2 = 0.12 ± 0.13. For the bottom graph, the best fit model was a four-exponential distribution function with corresponding dwell time and probability values (mean ± s.e.m.), as follows: τ_{off-1} = 1.06 ± 0.33 ms, P_1 = 0.63 ± 0.39, τ_{off-2} = 2.93 ± 1.74 ms, P_2 = 0.19 ± 0.31, τ_{off-3} = 13.67 ± 1.14 ms, P_3 = 0.13 ± 0.13, τ_{off-4} = 131.28 ± 1.19 ms, P_4 = 0.06 ± 0.05.

FBS-induced, large-amplitude blockades (ΔI_{HI-FBS}) were noted. The total frequency of HI-FBS-induced events at 12.63 nM Bs and 5% (v/v) HI-FBS was 0.14 ± 0.05 s^{-1} (n = 3). Notably, this value was much lower than that determined in the presence of 5% (v/v) FBS (4.48 ± 1.04 s^{-1}, n = 3). This

finding highlights the significance of the removal of FBS-induced residual blockades by HI of the serum. As in the case of FBS-incubated samples, the release and capture durations obeyed single-exponential event distributions (Supporting Information, Figure S11). Moreover, these time constants were independent of the HI-FBS concentration (Figure 3b; Supporting Information, Table S10). Therefore, we determined no statistically distinctive rate constants at increased HI-FBS concentrations. Finally, HI-FBS-induced events followed a multiexponential distribution that included four or less exponential terms (Figure 3c, Supporting Information, Tables S11−S13).

◾ DISCUSSION

In this article, we show single-molecule discrimination of proteins in FBS using a highly specific nanopore sensor. The detection readout is not acquired at the expense of protein unfolding,[29,30] because single-molecule capture events occur outside the nanopore[20,22,25] and they are accurately time resolved via discrete current transitions. Measurements using t-FhuA can be conducted at low salt concentrations,[13] elevated temperatures,[13] and increased osmotic pressures at a semi-dilute regime of crowding agents.[45] The polypeptide adaptor facilitates protein sensing outside the nanopore, a difficult process exacerbated by the fact that the dimensions of the folded, interacting proteins (e.g., bait and analyte) are greater than the cross-sectional diameter of the nanopore. Therefore, the adaptor enables the conversion of electrostatically driven Bs captures and releases into a high-fidelity electrical readout. This mechanism for protein detection is fundamentally distinct from those developed by our predecessors.[20,22,25,46] Previously, single-molecule protein detection has been conducted using protein nanopores equipped with small to medium-sized tethered ligands. Protein detection was also examined using solid-state nanopores by chemical attachment of protein recognition partners,[21,47] but the single-molecule precision of the attachment of these large functional protein groups remains difficult. Protein detection in FBS can be further optimized by making the nanopore even more acidic and measuring the protein captures at a lower positive potential (e.g., ~5 mV). The t-FhuA tolerates extensive alterations in the overall internal charge of the pore interior without affecting the stability of the open-state current.[48,49] Therefore, repelling a large amount of negatively charged FBS impurities by the more-acidic pore interior will likely be instrumental in pushing temporal resolution toward detection of weak-affinity protein analytes in FBS. Another opportunity for a reduction in FBS-induced noise is the use of the HI-FBS. Indeed, the frequency of FBS-induced irregular current blockades was drastically diminished by HI-FBS, suggesting that enhancement in the temporal resolution can be achieved. Other studies have highlighted the role of HI in enhancing protein detection.[43,44] Of course, this approach might only be used if the targeted protein analyte does not undergo denaturing under HI conditions.

In summary, we show quantitative protein detection in mammalian serum using a protein bait-containing biological nanopore. Measuring ion current modulation in the vicinity of the pore via a polypeptide tail adaptor is the most distinctive feature of this work from prior studies involving conventional nanopores. This process significantly differentiates our method from simple pore-plugging recordings, drastically enhancing its specificity. Because this selective nanopore sensor is

engineered in a modular fashion as a single-polypeptide chain protein, there is no requirement for tedious purification steps of the targeted oligomer from other products of the assembly reaction, as many other multimeric biological nanopores necessitate. Moreover, our method circumvents the need for chemical modification of the t-FhuA stem, as well as covalent attachment of fluorophores or other reactive groups. Finally, the ability to discriminate a specific protein from many others present in a heterogeneous solution will have a transformative impact on molecular biomedical diagnostics and protein biotechnology.

ASSOCIATED CONTENT

⑤ Supporting Information

The Supporting Information is available free of charge on the ACS Publications website at DOI: 10.1021/acssensors.9b00848.

> (i) Cloning and mutagenesis of the nanopore sensor and protein analyte; (ii) protein expression and purification; (iii) membrane protein refolding; (iv) single-molecule electrophysiology using planar lipid bilayers; (v) control single-channel electrical trace of the $OBn(GGS)_2$t-FhuA protein pore at −40 mV; (vi) standard histograms of the Bs capture and release events; (vii) FBS constituents produced long-lived current blockades at a high negative potential; (viii) voltage dependence of the differential current; (ix) the SNR of the O_{on} and O_{off} substates is improved at an applied transmembrane potential of +15 mV; (x) control single-channel electrical trace of the $OBn(GGS)_2$t-FhuA protein pore at +15 mV; (xi) standard histograms of the Bs capture and release events at +15 mV; (xii) analyses of the kinetic rate constants in homogeneous (FBS-free) and heterogeneous (FBS) solutions; (xiii) other pieces of Supporting Information; (xiv) supporting references (PDF)

AUTHOR INFORMATION

Corresponding Author

*E-mail: lmovilea@syr.edu. Phone: 315-443-8078. Fax: 315-443-9103.

ORCID ⓘ

Liviu Movileanu: 0000-0002-2525-3341

Author Contributions

A.K.T. and L.M. designed the research. A.K.T. performed the research and analyzed the data. A.K.T. and L.M. wrote the paper.

Notes

The authors declare the following competing financial interest(s): A.K.T. and L.M. are named inventors on one non-provisional patent application, US 16/177,554, filed by Syracuse University on this work.

REFERENCES

(1) Restrepo-Pérez, L.; Joo, C.; Dekker, C. Paving the way to single-molecule protein sequencing. *Nat. Nanotechnol.* **2018**, *13*, 786−796.

(2) Heikenfeld, J.; Jajack, A.; Feldman, B.; Granger, S. W.; Gaitonde, S.; Begtrup, G.; Katchman, B. A. Accessing analytes in biofluids for peripheral biochemical monitoring. *Nat. Biotechnol.* **2019**, *37*, 407−419.

(3) Wienken, C. J.; Baaske, P.; Rothbauer, U.; Braun, D.; Duhr, S. Protein-binding assays in biological liquids using microscale thermophoresis. *Nat. Commun.* **2010**, *1*, 100.

(4) Wang, S.; Haque, F.; Rychahou, P. G.; Evers, B. M.; Guo, P. Engineered nanopore of Phi29 DNA-packaging motor for real-time detection of single colon cancer specific antibody in serum. *ACS Nano* **2013**, *7*, 9814−9822.

(5) Fahie, M. A.; Yang, B.; Mullis, M.; Holden, M. A.; Chen, M. Selective Detection of Protein Homologues in Serum Using an OmpG Nanopore. *Anal. Chem.* **2015**, *87*, 11143−11149.

(6) Kukwikila, M.; Howorka, S. Nanopore-based electrical and label-free sensing of enzyme activity in blood serum. *Anal. Chem.* **2015**, *87*, 9149−9154.

(7) Yoo, J.; Lee, T.-S.; Choi, B.; Shon, M. J.; Yoon, T.-Y. Observing Extremely Weak Protein-Protein Interactions with Conventional Single-Molecule Fluorescence Microscopy. *J. Am. Chem. Soc.* **2016**, *138*, 14238−14241.

(8) Sze, J. Y. Y.; Ivanov, A. P.; Cass, A. E. G.; Edel, J. B. Single molecule multiplexed nanopore protein screening in human serum using aptamer modified DNA carriers. *Nat. Commun.* **2017**, *8*, 1552.

(9) Thakur, A. K.; Larimi, M. G.; Gooden, K.; Movileanu, L. Aberrantly Large Single-Channel Conductance of Polyhistidine Arm-Containing Protein Nanopores. *Biochemistry* **2017**, *56*, 4895−4905.

(10) Thakur, A. K.; Movileanu, L. Real-Time Measurement of Protein-Protein Interactions at Single-Molecule Resolution using a Biological Nanopore. *Nat. Biotechnol.* **2019**, *37*, 96−101.

(11) Locher, K. P.; Rees, B.; Koebnik, R.; Mitschler, A.; Moulinier, L.; Rosenbusch, J. P.; Moras, D. Transmembrane Signaling across the Ligand-Gated FhuA Receptor. *Cell* **1998**, *95*, 771−778.

(12) Mohammad, M. M.; Howard, K. R.; Movileanu, L. Redesign of a plugged beta-barrel membrane protein. *J. Biol. Chem.* **2011**, *286*, 8000−8013.

(13) Mohammad, M. M.; Iyer, R.; Howard, K. R.; McPike, M. P.; Borer, P. N.; Movileanu, L. Engineering a Rigid Protein Tunnel for Biomolecular Detection. *J. Am. Chem. Soc.* **2012**, *134*, 9521−9531.

(14) Liu, Z.; Ghai, I.; Winterhalter, M.; Schwaneberg, U. Engineering Enhanced Pore Sizes Using FhuA Delta1-160 from E. coli Outer Membrane as Template. *ACS Sens.* **2017**, *2*, 1619−1626.

(15) Wolfe, A. J.; Si, W.; Zhang, Z.; Blanden, A. R.; Hsueh, Y.-C.; Gugel, J. F.; Pham, B.; Chen, M.; Loh, S. N.; Rozovsky, S.; Aksimentiev, A.; Movileanu, L. Quantification of membrane protein-detergent complex interactions. *J. Phys. Chem. B* **2017**, *121*, 10228−10241.

(16) Schreiber, G.; Fersht, A. R. Interaction of barnase with its polypeptide inhibitor barstar studied by protein engineering. *Biochemistry* **1993**, *32*, 5145−5150.

(17) Deyev, S. M.; Waibel, R.; Lebedenko, E. N.; Schubiger, A. P.; Plückthun, A. Design of multivalent complexes using the barnase*-barstar module. *Nat. Biotechnol.* **2003**, *21*, 1486−1492.

(18) Buckle, A. M.; Schreiber, G.; Fersht, A. R. Protein-protein recognition: crystal structural analysis of a barnase-barstar complex at 2.0-A resolution. *Biochemistry* **1994**, *33*, 8878−8889.

(19) Larimi, M. G.; Mayse, L. A.; Movileanu, L. Interactions of a Polypeptide with a Protein Nanopore Under Crowding Conditions. *ACS Nano* **2019**, *13*, 4469−4477.

(20) Movileanu, L.; Howorka, S.; Braha, O.; Bayley, H. Detecting protein analytes that modulate transmembrane movement of a polymer chain within a single protein pore. *Nat. Biotechnol.* **2000**, *18*, 1091−1095.

(21) Wei, R.; Gatterdam, V.; Wieneke, R.; Tampé, R.; Rant, U. Stochastic sensing of proteins with receptor-modified solid-state nanopores. *Nat. Nanotechnol.* **2012**, *7*, 257−263.

(22) Rotem, D.; Jayasinghe, L.; Salichou, M.; Bayley, H. Protein Detection by Nanopores Equipped with Aptamers. *J. Am. Chem. Soc.* **2012**, *134*, 2781−2787.

(23) Jin, Q.; Fleming, A. M.; Johnson, R. P.; Ding, Y.; Burrows, C. J.; White, H. S. Base-excision repair activity of uracil-DNA glycosylase monitored using the latch zone of alpha-hemolysin. *J. Am. Chem. Soc.* **2013**, *135*, 19347−19353.

(24) Ying, Y.; Zhang, X.; Liu, Y.; Xue, M.; Li, H.; Long, Y. Single Molecule Study of the Weak Biological Interactions Between P53 and DNA. *Acta Chim. Sin.* **2013**, *71*, 44−50.

(25) Fahie, M.; Chisholm, C.; Chen, M. Resolved single-molecule detection of individual species within a mixture of anti-biotin antibodies using an engineered monomeric nanopore. *ACS Nano* **2015**, *9*, 1089−1098.

(26) Mohammad, M. M.; Movileanu, L. Excursion of a Single Polypeptide into a Protein Pore: Simple Physics, but Complicated Biology. *Eur. Biophys. J.* **2008**, *37*, 913−925.

(27) Niedzwiecki, D. J.; Grazul, J.; Movileanu, L. Single-molecule observation of protein adsorption onto an inorganic surface. *J. Am. Chem. Soc.* **2010**, *132*, 10816−10822.

(28) Bikwemu, R.; Wolfe, A. J.; Xing, X.; Movileanu, L. Facilitated Translocation of Polypeptides Through a Single Nanopore. *J. Phys.: Condens. Matter* **2010**, *22*, 454117.

(29) Nivala, J.; Marks, D. B.; Akeson, M. Unfoldase-mediated protein translocation through an *α*-hemolysin nanopore. *Nat. Biotechnol.* **2013**, *31*, 247−250.

(30) Rodriguez-Larrea, D.; Bayley, H. Multistep protein unfolding during nanopore translocation. *Nat. Nanotechnol.* **2013**, *8*, 288−295.

(31) Larkin, J.; Henley, R. Y.; Muthukumar, M.; Rosenstein, J. K.; Wanunu, M. High-bandwidth protein analysis using solid-state nanopores. *Biophys. J.* **2014**, *106*, 696−704.

(32) Kennedy, E.; Dong, Z.; Tennant, C.; Timp, G. Reading the primary structure of a protein with 0.07 nm3 resolution using a subnanometre-diameter pore. *Nat. Nanotechnol.* **2016**, *11*, 968−976.

(33) Yusko, E. C.; Bruhn, B. R.; Eggenberger, O. M.; Houghtaling, J.; Rollings, R. C.; Walsh, N. C.; Nandivada, S.; Pindrus, M.; Hall, A. R.; Sept, D.; Li, J.; Kalonia, D. S.; Mayer, M. Real-time shape approximation and fingerprinting of single proteins using a nanopore. *Nat. Nanotechnol.* **2017**, *12*, 360−367.

(34) Howorka, S. Building membrane nanopores. *Nat. Nanotechnol.* **2017**, *12*, 619−630.

(35) Wloka, C.; Van Meervelt, V.; van Gelder, D.; Danda, N.; Jager, N.; Williams, C. P.; Maglia, G. Label-Free and Real-Time Detection of Protein Ubiquitination with a Biological Nanopore. *ACS Nano* **2017**, *11*, 4387−4394.

(36) Hoogerheide, D. P.; Gurnev, P. A.; Rostovtseva, T. K.; Bezrukov, S. M. Real-Time Nanopore-Based Recognition of Protein Translocation Success. *Biophys. J.* **2018**, *114*, 772−776.

(37) Varongchayakul, N.; Song, J.; Meller, A.; Grinstaff, M. W. Single-Molecule Protein Sensing in a Nanopore: a Tutorial. *Chem. Soc. Rev.* **2018**, *47*, 8512−8524.

(38) Schreiber, G.; Fersht, A. R. Energetics of protein-protein interactions: analysis of the barnase-barstar interface by single mutations and double mutant cycles. *J. Mol. Biol.* **1995**, *248*, 478−486.

(39) Couoh-Cardel, S.; Hsueh, Y. C.; Wilkens, S.; Movileanu, L. Yeast V-ATPase Proteolipid Ring Acts as a Large-conductance Transmembrane Protein Pore. *Sci. Rep.* **2016**, *6*, 24774.

(40) Sackmann, B.; Neher, E. *Single-Channel Recording*, 2nd ed.; Kluwer Academic/Plenum Publishers: New York, 1995.

(41) Soltis, R. D.; Hasz, D.; Morris, M. J.; Wilson, I. D. The effect of heat inactivation of serum on aggregation of immunoglobulins. *Immunology* **1979**, *36*, 37−45.

(42) Cancado, E. L.; Vilas-Boas, L. S.; Abrantes-Lemos, C. P.; Novo, N. F.; Porta, G.; Da Silva, L. C.; Laudanna, A. A. Heat serum inactivation as a mandatory procedure for antiactin antibody detection in cell culture. *Hepatology* **1996**, *23*, 1098−1104.

(43) Namekar, M.; Kumar, M.; O'Connell, M.; Nerurkar, V. R. Effect of serum heat-inactivation and dilution on detection of anti-WNV antibodies in mice by West Nile virus E-protein microsphere immunoassay. *PLoS One* **2012**, *7*, e45851.

(44) Kennedy, S. N.; Wilhite, B.; Margaret Castellini, J.; Rea, L. D.; Kuhn, T. B.; Ferrante, A.; O'Hara, T. M. Enhanced quantification of serum immunoglobulin G from a non-model wildlife species, the Steller sea lion (Eumetopias jubatus), using a protein A ELISA. *J. Immunol. Methods* **2018**, *462*, 42−47.

(45) Niedzwiecki, D. J.; Mohammad, M. M.; Movileanu, L. Inspection of the Engineered FhuA deltaC/delta4L Protein Nanopore by Polymer Exclusion. *Biophys. J.* **2012**, *103*, 2115−2124.

(46) Harrington, L.; Cheley, S.; Alexander, L. T.; Knapp, S.; Bayley, H. Stochastic detection of Pim protein kinases reveals electrostatically enhanced association of a peptide substrate. *Proc. Natl. Acad. Sci. U.S.A.* **2013**, *110*, E4417−E4426.

(47) Ying, Y.-L.; Yu, R.-J.; Hu, Y.-X.; Gao, R.; Long, Y.-T. Single antibody-antigen interactions monitored via transient ionic current recording using nanopore sensors. *Chem. Commun.* **2017**, *53*, 8620−8623.

(48) Wolfe, A. J.; Mohammad, M. M.; Thakur, A. K.; Movileanu, L. Global redesign of a native *β*-barrel scaffold. *Biochim. Biophys. Acta* **2016**, *1858*, 19−29.

(49) Wolfe, A. J.; Hsueh, Y.-C.; Blanden, A. R.; Mohammad, M. M.; Pham, B.; Thakur, A. K.; Loh, S. N.; Chen, M.; Movileanu, L. Interrogating Detergent Desolvation of Nanopore-Forming Proteins by Fluorescence Polarization Spectroscopy. *Anal. Chem.* **2017**, *89*, 8013−8020.